Journal of Power Sources 251 (2014) 344–350

Contents lists available at ScienceDirect

Journal of Power Sources

journal homepage: www.elsevier.com/locate/jpowsour

Superior cycle stability and high rate capability of Zn–Al–In-hydrotalcite as negative electrode materials for Ni–Zn secondary batteries

Ruijuan Wang [a], Zhanhong Yang [a,b,*], Bin Yang [a], Tingting Wang [a], Zhihao Chu [a]

[a] College of Chemistry and Chemical Engineering, Central South University, Changsha 410083, China
[b] Key Laboratory of Resource Chemistry of Nonferrous Metals, Ministry of Education, Central South University, Changsha 410083, China

HIGHLIGHTS

- Zn–Al–In layered double hydroxides (LDHs) are synthesized by hydrothermal method.
- Zn–Al–In-LDHs have superior electrochemical cycle stability.
- Zn–Al–In-LDHs exhibits high discharge capability and long cycle life.
- Zn–Al–In-LDHs possess high rate capability.

ARTICLE INFO

Article history:
Received 10 September 2013
Received in revised form
14 November 2013
Accepted 19 November 2013
Available online 1 December 2013

Keywords:
Layered double hydroxides
Nickel–Zinc secondary batteries
Long cycle life
High discharge capacity
High rate capability

ABSTRACT

Zn–Al–In layered double hydroxides (LDHs) are synthesized by hydrothermal method and investigated as negative electrode materials for Ni–Zn batteries. The Fourier transform infrared spectra (FT-IR), X-ray diffraction (XRD), scanning electron microscopy (SEM) and transmission electron microscopy (TEM) images show the as-prepared samples are well-crystallized and hexagon structure. The electrochemical performances of Zn–Al-LDHs and Zn–Al–In-LDHs with different Zn/Al/In molar ration are investigated by the cyclic voltammograms (CV), Tafel polarization and galvanostatic charge–discharge measurements. Zn–Al-LDHs shows good stability in the first 300-cycles. However, during the subsequent cycles, the discharge capacity decreases with increasing of the cycles. Compared with Zn–Al-LDHs, Zn–Al–In-LDHs with different Zn/Al/In molar rations, especially the sample of Zn/Al/In = 3:0.75:0.25 (molar ration) have higher discharge capacity and more stable cycling performances. This battery can undergo at least 800 charge–discharge cycles at constant current of 1C without dendrite and short circuits. The discharge capacity of Zn–Al–In-LDHs after the 800th cycle remains about 380 mAh g^{-1}. Zn–Al–In-LDHs possess a high rate capability to meet the needs of high-storage applications.

1. Introduction

In recent years, there is an overwhelming need for a reliable, stable and cost effective energy storage device for applications ranging from large-scale energy storage to electric and hybrid vehicle applications. Widely used in the market of the lead-acid battery has serious polluting to the environment. The Nickel–Zinc alkaline secondary batteries with an operating voltage of ~1.765 V and the battery holds an almost constant voltage during most of the discharge period and exhibits voltage stability at different discharge rates. In addition, raw materials of the Nickel–Zinc battery are in rich and environmental friendly [1]. Therefore, Ni–Zn alkaline secondary battery is a promising candidate for the new generation of green power sources used in electric vehicle in recent years. However, the secondary zinc batteries are usually limited in widespread commercialization by the poor cycle life and inferior discharge performance. The failure is usually caused by the drawbacks of zinc electrode, such as zinc dendrite, zinc self-corrosion and shape change in charge–discharge processes [2]. The problems mainly derive from a high solubility of zinc active material in alkaline electrolyte. Hence, many attempts have been made to conquer the problems, most of researchers have focused on the electrolyte, modification of ZnO and additives in the electrodes.

So far, a large variety of additives, such as $Ca(OH)_2$ [3,4], Bi_2O_3 [5–7], $In(OH)_3$ [8–10], BaO [11], were used in zinc electrodes to

* Corresponding author. Tel./fax: +86 731 88879616.
E-mail addresses: zhyang@mail.csu.edu.cn, zhongnan320@gmail.com (Z. Yang).

0378-7753/$ – see front matter © 2013 Elsevier B.V. All rights reserved.
http://dx.doi.org/10.1016/j.jpowsour.2013.11.071

overcome the problems mentioned above and an obvious enhancement has been obtained. Among all these additives, compounds of indium are thought to be the important component of electrode due to these compounds have a suppressive effect on H_2 formation, decrease shape change and self-discharge, resulting in a more uniform current density distribution and improved cell lifetimes [9].

LDHs, or hydrotalcite-like compounds, are a class of anionic clays consisting of positively charged metal hydroxide layers with charge-compensating anions located in the interlayer, with the general formula $[M(II)_{1-x}M(III)_x(OH)_2]^{x+}(A^{n-})_{x/n}\cdot mH_2O$, while M(II) is a divalent metal cation, M(III) is a trivalent metal, and A^{n-} is an anion [12]. LDHs has been applied in many aspects, including catalysts [13–15], ion conductivity [16,17], adsorbents [18–21] and anion exchangers [22–25]. Zn–Al-hydrotalcite have been directly applied to the zinc electrode by our previous work [10,26,27], and the results show Zn–Al-hydrotalcite as anodic materials of Ni–Zn batteries exhibits good reversibility, superior electrochemical cycling stability and more excellent utilization ration in the alkaline solution compared with the ZnO. However, Zn–Al-LDHs suffer low conductivity and largely suppress the electron transfer for electrode reaction [10]. Therefore, in order to enhance its electrochemical performances, it should be further modification on Zn–Al-LDHs. In the present work, Zn–Al–In-LDHs have been proposed as zinc electrode materials and the electrochemical properties were studied in details by us [28].

2. Experimental

2.1. The preparation of Zn–Al–In-hydrotalcites

The Zn–Al–In-hydrotalcites (Zn–Al–In-LDHs) were prepared by a hydrothermal method. An aqueous solution (100 ml) of Zn, Al and In nitrates (with Zn: Al: In molar ratio equal to 3:1:0, 4:0.8:0.2, 3:0.75:0.25, 2:0.67:0.33) and total metal ion concentration of 0.25 mol L^{-1} was added with flow rate of 5 ml min^{-1} into batch reactor containing 50 ml of distilled water. The flow rate of simultaneously added alkaline solution (100 ml) of Na_2CO_3 (0.0125 mol) and NaOH (0.05 mol) was controlled to maintain the reaction pH of 10. The process was carried out under vigorous stirring at 45 °C, then transferred the above reaction solution to a reaction kettle and continually stirred for 10 min, then sealed the kettle and kept it in thermostatic drying closet, reacting at 120 °C for ten hours, filtering, washing and vacuum drying at 60 °C, then the product of Zn–Al–In-LDHs powders were collected and packed in a PE bag for further examination and use.

2.2. The characterization of the Zn–Al–In-LDHs samples

Fourier transform infrared spectra (FT-IR) of the samples were conducted on a Nicolet Nexus-670 FT-IR spectrometer (as KBr discs, with wave number 400–4000 cm^{-1}, resolution 0.09 cm^{-1}, and the weight of measured sample is 2 mg). XRD patterns of samples were recorded by a D500 (Siemens) diffractometer (36 kV, 30 mA) using Cu Kα radiation at a scanning rate of $2\theta = 8°$ min^{-1}. The morphology of the Zn–Al–In-LDHs products was examined by SEM (JSM-6360LV) and TEM (JEM-2100F).

2.3. The preparation and electrochemical measurements of the Zn–Al–In-LDHs electrodes

The Zn–Al–In-LDHs electrodes were prepared by incorporation slurries containing 85 wt.% Zn–Al–In-LDHs, 10 wt.% acetylene black and 5 wt.% additives of polytetrafluoroethylene (PTFE, 60 wt.%, in diluted emulsion). Copper mesh (1.0 cm × 1.0 cm in size) was served as the current collector and the Zn–Al–In-LDHs electrodes were roll-pressed to a thickness of 0.2 mm. Then, the obtained Zn–Al–In-LDHs electrodes were dried at 60 °C under vacuum. For comparison, Zn–Al-LDH electrodes composed of Zn–Al-LDHs were also fabricated by the same way. The positive electrode was the commercial sintered $Ni(OH)_2$ electrode (Tianjin City Fine Chemical Research Institute) whose capacity was much larger than Zn–Al–In-LDHs electrode for making full use of the active material in Zn–Al–In-LDHs electrode. The electrolyte is solution of 6 M KOH saturated with ZnO. All the cells were pre-activated for 10 times by the following operations: The cells were charged at constant current of 1C for 60 min, and discharged at constant current of 1C to a cut-off voltage of 1.2 V.

A three-electrode cell was assembled for cyclic voltammograms (CV) and Tafel polarization, with Hg/HgO electrode served as the reference electrode, pre-activated pasted zinc electrode as the working electrode and the sintered Nickel electrode as counter electrode. The capacity of counter electrode was far higher than that of zinc electrode. The electrolyte was 6 mol L^{-1} KOH solution saturated with ZnO. CV was carried out on an electrochemical workstation (CHI660D) at room temperature at a scanning rate of 5 mV s^{-1} range from −0.8 V to −1.8 V. Tafel polarization curves were carried out using an electrochemical workstation (RST-500) at room temperature with a scanning rate of 0.5 mV s^{-1}. The galvanostatic charge–discharge tests were performed on a BTS-5 V/10 mA battery-testing instrument (Neware, China) at room temperature. During the cycling process, the cells were charged at 1C for 60 min and discharged at 1C down to 1.2 V cut-off voltages.

In all the above experiments, the reagents used were A.R. grade and the electrolyte was prepared with deionized water.

3. Results and discussions

3.1. The structural analysis of Zn–Al–In-LDHs

For the samples of Zn–Al-LDHs and Zn–Al–In-LDHs with different Zn/Al/In molar ratio, the FT-IR spectra are shown in Fig. 1. The broad band around 3440.78 cm^{-1} corresponds to the stretching vibrations of hydroxyl groups attached to metal ions. The prominent absorption bands (1505.19 cm^{-1} and 1364.61 cm^{-1}) due to C–O asymmetric stretching, a considerably lower shifted absorption peak at 1364.61 cm^{-1}, as compared with CO_3^{2-} of $CaCO_3$

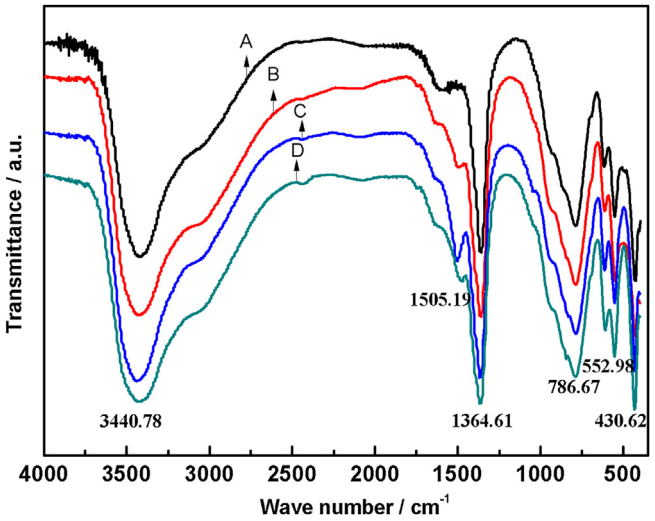

Fig. 1. FT-IR spectra of Zn–Al-LDHs and different Zn/Al/In molar rations of Zn–Al–In-LDHs, A: Zn/Al/In = 3:1:0; B: Zn/Al/In = 4:0.8:0.2; C: Zn/Al/In = 3:0.75:0.25; D: Zn/Al/In = 2:0.67:0.33.

(1430 cm^{-1}), shows that there was an intercalation between CO_3^{2-} and interlayer H_2O through the strong hydrogen bonding. The lower wave number bands at 400–700 cm^{-1} is due to LDH lattice vibrations (Zn–O, Al–O, In–O). The bands at 786.67 cm^{-1}, 552.98 cm^{-1} and 430.62 cm^{-1} can be assigned to the Al–O stretching modes and In–O. These peaks intensity are not weakened compared with those of Zn–Al-LDHs, indicating Aluminum atoms in lattice can be replaced by Indium atoms effectively and these bonds are not damaged.

XRD patterns of the as-prepared Zn–Al-LDHs and Zn–Al–In-LDHs with different Zn/Al/In molar ratio are shown in Fig. 2. As seen in Fig. 2, the diffraction peaks at 2θ = 11.7°, 23.56°, 34.56° and 61.56° corresponding to (003), (006), (009) and (110) planes, respectively, which can also be seen in that of Zn–Al–In-LDHs. The highest diffraction peak of the four kinds of as-prepared samples appears at $2\theta = 11.7°$, suggesting Zn–Al-LDHs and all three kinds of Zn–Al–In-LDHs are highly crystallized hydrotalcite-like compound and a typical hexagonal crystal structure [26]. The diffraction peaks are shape, narrow and symmetrical, with a low and stable baseline, indicating that all the samples are well-crystallized. As observed, there are some weak peaks of sample D comparing with other samples, indicating the excessive indium additive leads to disproportion of lattice which impacts crystallization of Zn–Al–In-LDHs. Compared with sample B, the highest diffraction peak at $2\theta = 11.7°$ of sample C are stronger, which shows that the right amount of indium atoms are replaced effectively, and the homogeneously dispersed indium atoms are beneficial to Zn–Al–In-LDHs good crystallization.

As shown in Fig. 3a, the existing lamellar Zn–Al–In-LDHs particles have hexagon layer structure, which is the typical structure of the hydrotalcite-like material [29]. The particle size of Zn–Al–In-LDHs is about 200–400 nm, and the lamellar thickness is about 70 nm. Fig. 3b shows the TEM image of highly crystalline Zn–Al–In-LDHs sample. As can be seen, the sample typically consists of the hexagon layer structure with a size about 200–400 nm.

3.2. The cyclic voltammograms of Zn electrodes

In order to investigate the electrochemical performance of the Zn–Al-LDHs and Zn–Al–In-LDHs, CV studies were carried out and the recorded CV curves are shown in Fig. 4. The curves should be associated with Zn^{2+}/Zn redox couple and the reaction have been reported by us [27]. As observed from Fig. 4, the cathodic peaks potential of zinc electrodes containing the Zn–Al-LDHs (code A), Zn–Al–In-LDHs with Zn:Al:In = 4:0.8:0.2 (code B), Zn–Al–In-LDHs with Zn:Al:In = 3:0.75:0.25 (code C), Zn–Al–In-LDHs with Zn:Al:In = 2:0.67:0.33 (code D) appear at −1.611 V, −1.607 V, −1.600 V and −1.602 V, respectively. The cathodic peak corresponds to the charging process. During the charging process, zinc ions free out from the structure of the hydrotalcite in the first step and then reduced into zinc metal. The possible reaction can be represented by Equations (1)–(3).

$$[Zn_{1-x-y}Al_xIn_y(OH)_2]^{(x+y)^+}(CO_3)^{2n^-}_{(\frac{x+y}{2n})}\cdot mH_2O \rightarrow (1-x-y)Zn^{2+} + xAl^{3+} + yIn^{3+} + 2OH^- + \left(\frac{x+y}{2n}\right)CO_3^{2n^-} + mH_2O \quad (1)$$

$$Zn^{2+} + 4OH^- \rightarrow Zn(OH)_4^{2-} \quad (2)$$

$$Zn(OH)_4^{2-} + 2e \rightarrow Zn + 4OH^- \quad (3)$$

Their corresponding anodic peaks potential at −1.034 V, −1.075 V, −1.101 V and −1.081 V are also observed in Fig. 4. During the discharging process, zinc metal is oxidized into bivalent zinc ions, and then the bivalent zinc ions enter into the structure of hydrotalcite. So the discharge products are Zn–Al–In-LDHs. However, expect most of Zn metal is oxidized into Zn–Al–In-LDHs, there are some Zn metal is oxidized into the byproduct-ZnO, which have been exploited by us [28]. The oxidation reaction can be represented by Equation (4).

$$Zn + 4OH^- \rightarrow Zn(OH)_4^{2-} + 2e \quad (4)$$

The potential interval between an anodic peak and a cathodic peak is taken as a measurement of the reversibility of the electrode reaction, and the smaller the interval, the better the reversibility. The potential interval of Zn–Al-LDHs is wider than Zn–Al–In-LDHs and the Zn–Al–In-LDHs with Zn:Al:In = 3:0.75:0.25 with the smallest potential interval of 0.499 V, which means the Zn–Al-LDHs has weaker reversibility of the electrode reaction than Zn–Al–In-LDHs and electrode C has the better reversibility. The better reversibility is attributed to the indium additive in the Zn–Al–In-LDHs. The high hydrogen evolution over-potential of indium atoms can inhibit hydrogen evolution reaction of Zn–Al–In-LDHs electrode, resulting in good reversibility. The different reversibility of the three kinds of Zn–Al–In-LDHs electrodes is ascribed to the concentration of indium metal in the four kinds of hydrotalcite. The less amount of In additive cannot effectively suppress H_2 formation. Because of the atomic radius of In is larger than that of Al, an excessive In additive leads to disproportion of lattice which impacts zinc atoms contact with electrolyte and reduces the electrochemical activity [27]. The anodic process reflects the discharge process of Ni–Zn secondary battery. The relatively negative anodic peak potential shows the discharge process of zinc electrode C can occur in lower potential, so Ni–Zn batteries with electrode C delivers higher discharge voltage. The better electrochemical performance of electrode C is attributed to the appropriate amount of In atoms are replaced homogeneously, which not only increase electrochemical activity, but also effectively suppress H_2 formation. The less amount of In additive cannot effectively suppress H_2 formation and the excessive In additive reduces the electrochemical activity.

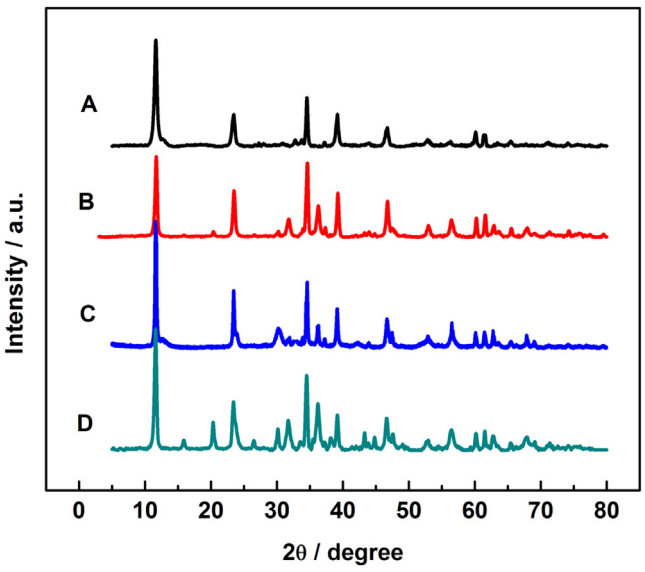

Fig. 2. XRD patterns of Zn–Al-LDHs and different Zn/Al/In molar rations of Zn–Al–In-LDHs, A: Zn/Al/In = 3:1:0; B: Zn/Al/In = 4:0.8:0.2; C: Zn/Al/In = 3:0.75:0.25; D: Zn/Al/In = 2:0.67:0.33.

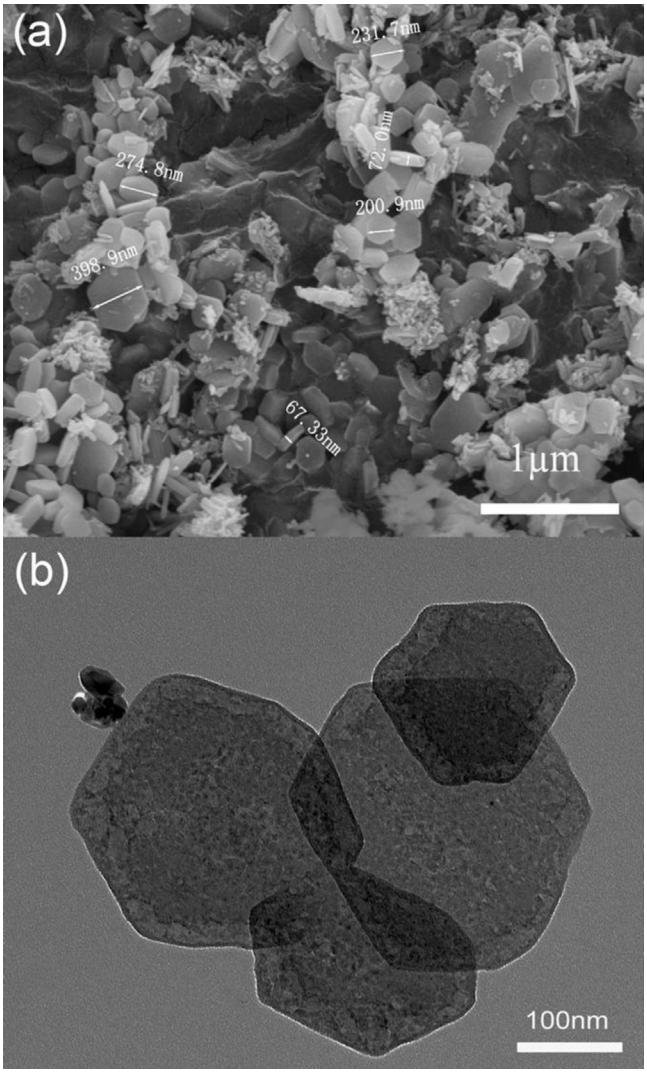

Fig. 3. SEM (a) and TEM (b) images of Zn–Al–In-LDHs with Zn/Al/In = 3:0.75:0.25.

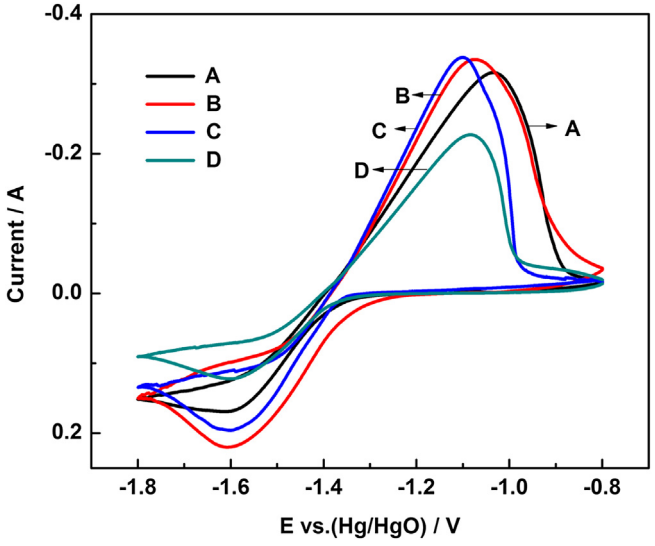

Fig. 4. Cyclic voltammograms for zinc electrodes with Zn–Al-LDHs and different Zn/Al/In molar rations of Zn–Al–In-LDHs, A: Zn/Al/In = 3:1:0; B: Zn/Al/In = 4:0.8:0.2; C: Zn/Al/In = 3:0.75:0.25; D: Zn/Al/In = 2:0.67:0.33.

3.3. The Tafel polarization curves of zinc electrodes

For understanding the changes of corrosion protection properties of Zn–Al–In-LDHs on the performance of zinc electrode, the Tafel polarization experiments are carried out. Fig. 5 shows the experimental results from the polarization curves of zinc electrodes without or with the indium additive of different ration. The electrochemical kinetic parameters derive from these curves are given in Table 1. The electrochemical kinetic parameters include corrosion potential (E_{corr}), corrosion current density (I_{corr}), and inhibition efficiency (I.E.%). The inhibition efficiency expressed as percent inhibition I.E.% is defined as formula (5) [30].

$$\text{I.E.\%} = \frac{I^0_{corr} - I_{corr}}{I^0_{corr}} \times 100 \quad (5)$$

I^0_{corr} and I_{corr} are the uninhibited and inhibited corrosion currents. As observed, the polarization curves of Zn–Al–In-LDHs electrodes are shifted to slightly larger corrosion potential and lower corrosion current compared to Zn–Al-LDH electrode, thus demonstrating Zn–Al–In-LDHs electrodes have a better corrosion resistance. As observed from Table 1, the three kinds of Zn–Al–In-LDHs exhibit positive steady-state corrosion potential and low corrosion current. The high inhibition efficiency of the Zn–Al–In-LDHs electrode may be attributed to the indium additive. Indium metal with high over-potential of hydrogen evolution, make zinc anode hydrogen evolution over-potential shift positively, suppresses the corrosion of zinc anode in the high concentration of alkaline electrolyte. Moreover, the inhibition efficiency of Zn–Al–In-LDHs with Zn:Al:In = 3:0.75:0.25 is the greatest, and the steady-state corrosion potential is the most positive. For the Zn–Al–In-LDHs with Zn:Al:In = 4:0.8:0.2, the In_2O_3 amount of the formation is relatively few due to the adding less amount of In which cannot effectively make zinc anode hydrogen evolution over-potential shift positively. The Tafel empirical formula is described as following

$$\eta_{H_2} = a + b \log j \quad (6)$$

η_{H_2} – hydrogen evolution over-potential
a – constant value related to electrode materials
b – constant value of 0.116 V
j – corrosion current.

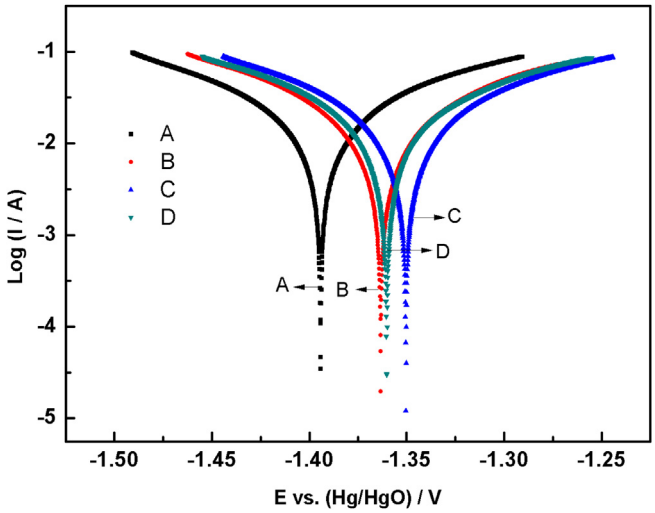

Fig. 5. Tafel polarization curves for zinc electrodes with Zn–Al-LDHs and different Zn/Al/In molar rations of Zn–Al–In-LDHs, A: Zn/Al/In = 3:1:0; B: Zn/Al/In = 4:0.8:0.2; C: Zn/Al/In = 3:0.75:0.25; D: Zn/Al/In = 2:0.67:0.33.

Table 1
The data for the Tafel curves for zinc electrodes with Zn–Al-LDHs and different Zn/Al/In molar rations of Zn–Al–In-LDHs, A: Zn/Al/In = 3:1:0; B: Zn/Al/In = 4:0.8:0.2; C: Zn/Al/In = 3:0.75:0.25; D: Zn/Al/In = 2:0.67:0.33.

Sample	E_{corr} (V)	I_{corr} (mA cm^{-2})	I.E.%
A	−1.3942	2.04×10^{-2}	–
B	−1.3634	1.75×10^{-2}	14.2
C	−1.3507	1.68×10^{-2}	17.6
D	−1.3603	1.82×10^{-2}	9.9

As described above, the excessive In additive makes disproportion of lattice, and the uneven crystal lattice reduces the value of the constant "*a*". So the hydrogen evolution over-potential of Zn–Al–In-LDHs with Zn:Al:In = 2:0.67:0.33 is smaller. In conclusion, Zn–Al–In-LDHs with Zn:Al:In = 3:0.75:0.25 possess the larger hydrogen evolution over-potential. The higher hydrogen evolution over-potential can inhibit hydrogen evolution reaction of Zn–Al–In-LDHs electrode, so that the corrosion of Zn–Al–In-LDHs electrode can be slowed on alkaline solution.

3.4. The properties of galvanostatic charge and discharge

The galvanostatic charge and discharge curves of Ni–Zn batteries using the Zn–Al-LDHs and Zn–Al–In-LDHs electrodes at the 50th cycle are displayed in Fig. 6. The overall electrode reaction can be described as Equations (7) and (8) [26,27].

Charge process

$$Zn(OH)_4^{2-} + 2e \rightarrow Zn + 4OH^- \quad (7)$$

Discharge process

$$Zn + 4OH^- \rightarrow Zn(OH)_4^{2-} + 2e \quad (8)$$

From Fig. 6, it can be seen that Ni–Zn battery with electrodes B, C and D present a lower charge and higher discharge plateau than that of the Zn–Al-LDHs. The decrease in charge plateau voltage is advantage to the suppression of H_2 formation and improvement of charge efficiency, and the high discharge plateau means high output energy and power [31]. The suppression of H_2 formation is attributed to the higher hydrogen evolution over-potential of indium metal in the Zn–Al–In-LDHs [27]. Furthermore, higher discharge plateau voltage associates with higher discharge potential and better performance in discharge process. As observed from Fig. 6, batteries B, C and D exhibit better discharge performance. This is explained by the sufficient electrical contact result from indium metal in the Zn–Al–In-LDHs particles. Meanwhile, the decrease in discharge plateau voltage indicates that indium hydroxide in the Zn–Al–In-LDHs gives a suppressive effect on electrochemical oxidized reactions of Zn. This suppressive effect would decrease the direct contact between zinc active materials and electrolyte. However, it could be noted that a decrease in discharge plateau voltage has no undesirable influence on discharge specific capacity of Ni–Zn batteries. This lie in the fact that Zn–Al–In-LDHs only suppresses electrochemical reaction rate to a certain extent and leads to a lower electrochemical kinetics, which is favorable to keep the electrochemical stability of zinc electrodes [9,32]. Furthermore, compared with batteries B and D, battery C shows the lowest discharge plateau voltage. This means Zn–Al–In-LDHs with Zn:Al:In = 3:0.75:0.25 shows the best electrochemical performances, which is consistent with the CV performance of the zinc electrodes shown in Fig. 4.

3.5. The cycle performance analysis of Zn–Al–In-LDHs

The long-term cycling stability was evaluated with Zn–Al-LDHs and Zn–Al–In-LDHs as anode materials. The batteries were charged and discharged for 800 cycles at current density of 1C as shown in Fig. 7. As shown in Fig. 7, it can be found that all the three kinds of Zn–Al–In-LDHs electrodes show more excellent cycle stability in the 800 cycles. In the first 300 cycles, Zn–Al-LDHs battery exhibits good cycle stability. However, during the subsequent cycles, the discharge capacity of Zn–Al-LDHs decreased with increasing charge–discharge cycles. In the 800-cycles, for the three kinds of batteries with Zn–Al–In-LDHs, its discharge specific capacity relatively stable and the discharge capacity are all about 380 mAh g^{-1}. Nevertheless, the discharge capacity of Zn–Al-LDHs battery reduced to 160 mAh g^{-1}. Compared with the other zinc

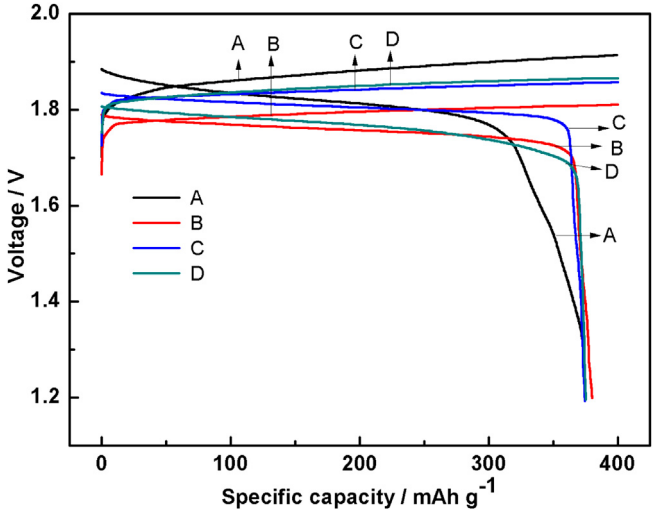

Fig. 6. Typical galvanostatic charge–discharge curves of Nickel–Zinc secondary batteries with Zn–Al-LDHs and different Zn/Al/In molar rations of Zn–Al–In-LDHs, A: Zn/Al/In = 3:1:0; B: Zn/Al/In = 4:0.8:0.2; C: Zn/Al/In = 3:0.75:0.25; D: Zn/Al/In = 2:0.67:0.33.

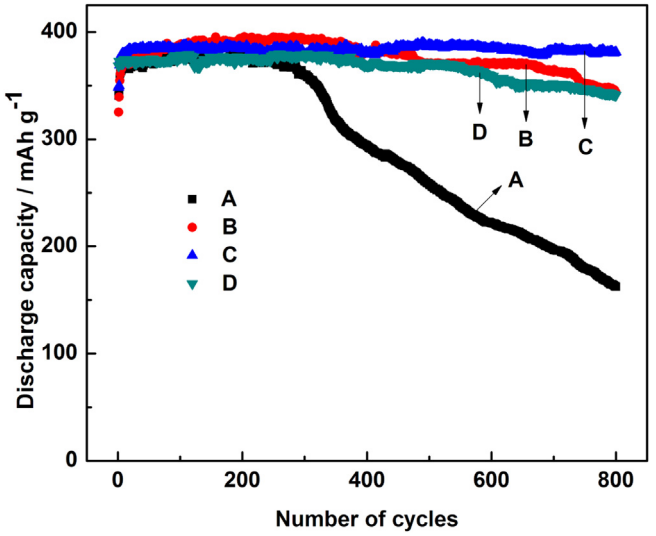

Fig. 7. Electrochemical cycle behavior of Nickel–Zinc secondary batteries with Zn–Al-LDHs and different Zn/Al/In molar rations of Zn–Al–In-LDHs, A: Zn/Al/In = 3:1:0; B: Zn/Al/In = 4:0.8:0.2; C: Zn/Al/In = 3:0.75:0.25; D: Zn/Al/In = 2:0.67:0.33.

active materials [8], LDHs has the relatively good cycle life. Moreover, the above results demonstrate that the battery with Zn–Al–In-LDHs shows a better stability and longer cycle life than that of Zn–Al-LDHs. The main reasons are generally attributed to the typical layer structure of LDHs and the existence of indium elements [28].

In conclusion, Zn–Al–In-LDHs present a superior cycle performance as anode materials for Ni–Zn secondary batteries, and electrode C exhibits the best electrochemical performance. In order to further illuminate the electrochemical performance of Zn–Al–In-LDHs, the electrochemical stability of Zn–Al–In-LDHs with Zn:Al:In = 3:0.75:0.25 is confirmed by the following cycle tests.

To further determine the cycle stability of the battery, the voltage profiles of the electrodes for various cycles are illustrated in Fig. 8. It can be observed that the four cycles exhibit similar charge and discharge curves, and the average change in the charge and discharge voltages with the cycle number is extremely little, and slight polarization or degradation is observed. The average charge voltage are 1.812 V (100th), 1.831 V (300th), 1.834 V (500th) and 1.841 V (800th) respectively. The average discharge voltage are 1.788 V (100th), 1.798 V (300th), 1.795 V (500th) and 1.796 V (800th) respectively. Since the increase in polarization by the long cycle (800 cycles) charge–discharge of Zn–Al–In-LDHs cells is very small, it is suggested that the Zn–Al–In-LDHs are stable under dynamic (charge–discharge) condition. Therefore, it is reasonable to conclude that the stable electrochemical reactions take place without any side reactions. Therefore, the Zn–Al–In-LDHs with Zn:Al:In = 3:0.75:0.25 exhibits the good cycle stability.

3.6. The rate performances analysis of Zn–Al–In-LDHs

A high rate capability is more important in meeting the needs of high-storage applications [33]. So the rate capability is an important standard for measuring the performance for Ni–Zn battery. In order to measuring the rate capability of Zn–Al–In-LDHs, the batteries were cycled at various rate of 1C and 2C, and the results are shown in Figs. 9 and 10. Fig. 9 shows fifth charge–discharge curves of the Zn–Al–In-LDHs with Zn:Al:In = 3:0.75:0.25 at the various current densities (1C rate and 2C rate). The active materials were worked as a rechargeable electrode and exhibit the high discharge capacity over 380 mAh g^{-1}. Moreover, it exhibits the higher discharge capacity of 390 mAh g^{-1} at the high current of 2C rate. The size of polarization can be obtained by the charge voltage and discharge voltage difference. As observed from Fig. 9, the battery at the high current density of 2C rate have larger polarization. The polarization increases with the increasing of current rate, it is because the time for Zn^{2+} ion intercalation into the crystal lattice were reduced at high current. However, it also can be seen that the discharge capacity increases with the increase of the applied current density, indicating that the polarization not influence the discharge capacity. Fig. 10 shows cycle performances of the Zn–Al–In-LDHs with Zn:Al:In = 3:0.75:0.25 at the various constant current densities of 1C rate and 2C rate. Discharge capacity and cycle stability at the current density of 2C rate are superior to that at the current density of 1C rate. The high discharge capacity can be attributed to the larger energy density of the electrode at a higher current rate. As observed from Fig. 9, charge–discharge curves show larger polarization potential of reduction reaction (Equation (4)) at the higher current rate. The hydrogen evolution potential

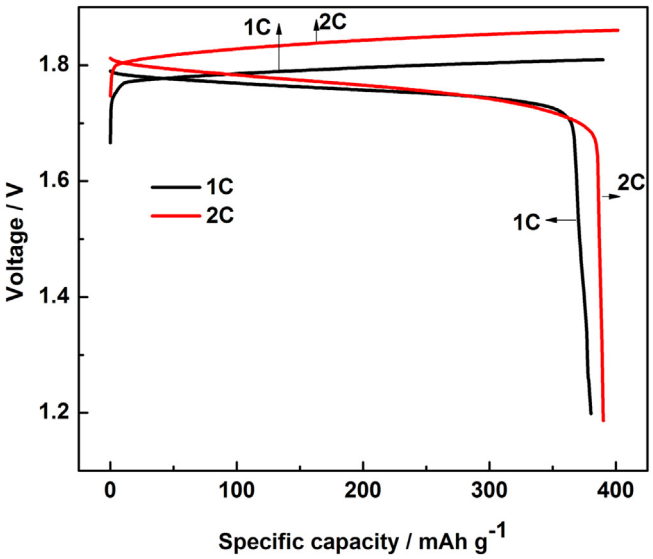

Fig. 9. The fifth charge–discharge curves of the Zn–Al–In-LDHs with Zn/Al/In = 3:0.75:0.25 at the various current densities (1C rate and 2C rate).

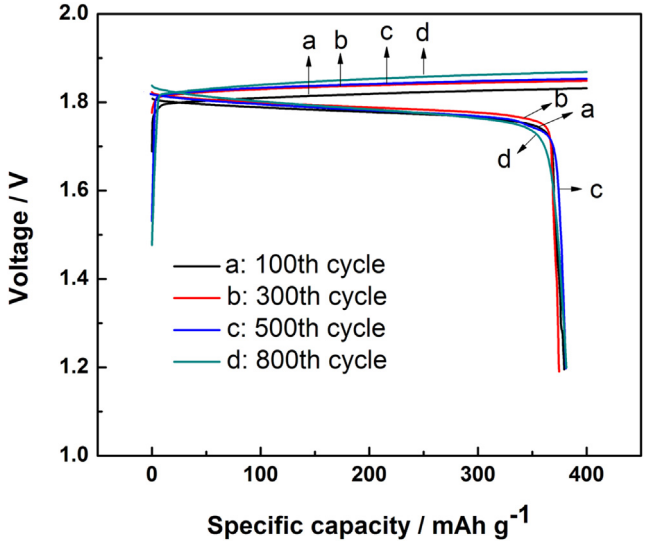

Fig. 8. The charge–discharge curves of Zn–Al–In-LDHs electrodes with Zn/Al/In = 3:0.75:0.25 at (a) 100th cycle, (b) 300th cycle, (c) 500th cycle and (d) 800th cycle.

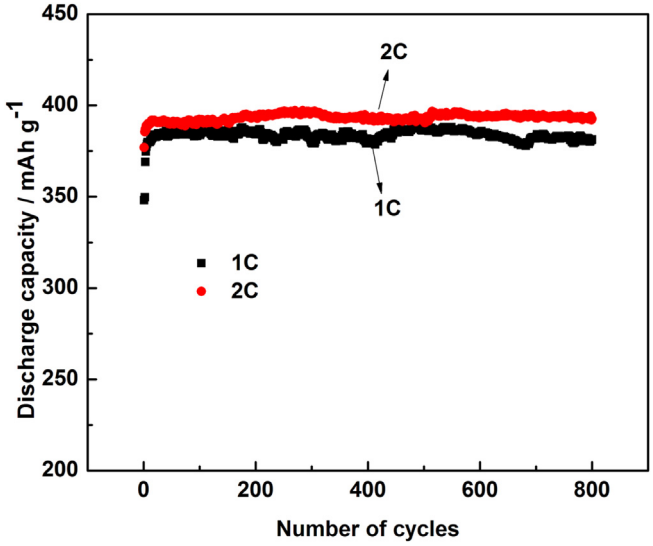

Fig. 10. Cycle performances of the Zn–Al–In-LDHs with Zn/Al/In = 3:0.75:0.25 at the constant current densities of 1C rate and 2C rate.

(φ_H) decreased due to the higher hydrogen evolution over-potential (η_H) of zinc anode caused by indium additive, and the formula is as following:

$$\varphi_H = \varphi_H^0 - \eta_H \quad (9)$$

φ_H – hydrogen evolution potential
φ_H^0 – electrode potential of hydrogen evolution reaction
η_H – hydrogen evolution over-potential.

Therefore, hydrogen evolution reaction will not occurred at the higher potential, leading to high conversion efficiency of electric energy into chemical energy. Consequently, the discharge capacity of the battery increased correspondingly. Thus, Zn–Al–In-LDHs not only exhibits good cycle performances, but also possess a high rate capability to meet the needs of high-storage applications.

4. Conclusions

Zn–Al-LDHs and Zn–Al–In-LDHs have been synthesized by hydrothermal method. The resulting Zn–Al–In-LDHs with different Zn/Al/In molar ration, especially the sample of Zn/Al/In = 3:0.75:0.25 (molar ration) employed as anode materials exhibit a better electrochemical performance compared with Zn–Al-LDHs. The Zn–Al–In-LDHs can effectively improve both the discharge capacity and the cycling stability. Zn–Al–In-LDHs possess a high rate capability to meet the needs of high-storage applications. These results provide important insights for develop a novel active materials with higher discharge capacity, good stability and high rate capability in Ni–Zn secondary batteries.

Acknowledgments

This work was supported by the Natural Science Foundation of China (Nos. 21371180 and 91023031), Science and Technology Project of Changsha City (Nos. K1303015-11 and K1203014-11) and Specialized Research Fund for the Doctoral Program of Higher Education (No. 20130162110018).

References

[1] J. Cheng, L. Zhang, Y. Yang, Y. Wen, G. Cao, X. Wang, Electrochem. Commun. 9 (2007) 2639–2642.
[2] J. Jindra, J. Power Sources 88 (2000).
[3] Y. Yuan, J. Tu, H. Wu, Y. Li, D. Shi, X. Zhao, J. Power Sources 159 (2006) 357–360.
[4] R. Wang, Z. Yang, B. Yang, X. Fan, T. Wang, J. Power Sources 246 (2014) 313–321.
[5] J. McBreen, E. Gannon, J. Power Sources 15 (1985) 169–177.
[6] Y.F. Yuan, Y. Li, S. Tao, F.C. Ye, J.L. Yang, S.Y. Guo, J.P. Tu, Electrochim. Acta 54 (2009) 6617–6621.
[7] Y.F. Yuan, L.Q. Yu, H.M. Wu, J.L. Yang, Y.B. Chen, S.Y. Guo, J.P. Tu, Electrochim. Acta 56 (2011) 4378–4383.
[8] S. Wang, Z. Yang, L. Zeng, J. Electrochem. Soc. 156 (2009) A18.
[9] D. Zeng, Z. Yang, S. Wang, X. Ni, D. Ai, Q. Zhang, Electrochim. Acta 56 (2011) 4075–4080.
[10] X. Fan, Z. Yang, W. Long, Z. Zhao, B. Yang, Electrochim. Acta 92 (2013) 365–370.
[11] Y. Zheng, J.M. Wang, H. Chen, J.Q. Zhang, C.N. Cao, Mater. Chem. Phys. 84 (2004) 99–106.
[12] T. Tamaki, N. Nakanishi, H. Ohashi, T. Yamaguchi, Electrochem. Commun. 25 (2012) 50–53.
[13] S. He, Z. An, M. Wei, D.G. Evans, X. Duan, Chem. Commun. (Camb.) 49 (2013) 5912–5920.
[14] P. Koilraj, K. Srinivasan, Ind. Eng. Chem. Res. 52 (2013) 7373–7381.
[15] J. Zhao, Y. Xie, W. Yuan, D. Li, S. Liu, B. Zheng, W. Hou, J. Mater. Chem. B 1 (2013) 1263.
[16] D. Kubo, K. Tadanaga, A. Hayashi, M. Tatsumisago, J. Electroanal. Chem. 671 (2012) 102–105.
[17] D. Kubo, K. Tadanaga, A. Hayashi, M. Tatsumisago, J. Power Sources 222 (2013) 493–497.
[18] A. Garcia-Gallastegui, D. Iruretagoyena, V. Gouvea, M. Mokhtar, A.M. Asiri, S.N. Basahel, S.A. Al-Thabaiti, A.O. Alyoubi, D. Chadwick, M.S.P. Shaffer, Chem. Mater. 24 (2012) 4531–4539.
[19] A. Halajnia, S. Oustan, N. Najafi, A.R. Khataee, A. Lakzian, Appl. Clay Sci. 70 (2012) 28–36.
[20] Q. Wang, Y. Gao, J. Luo, Z. Zhong, A. Borgna, Z. Guo, D. O'Hare, RSC Adv. 3 (2013) 3414.
[21] X. Yu, T. Luo, Y. Jia, R. Xu, C. Gao, Y. Zhang, J. Liu, X. Huang, Nanoscale 4 (2012) 3466–3474.
[22] Z. Liu, R. Ma, Minoru Osada, Nobuo Iyi, Yasuo Ebina, Kazunori Takada, Takayoshi Sasaki, J. Am. Chem. Soc. 128 (2006) 4872–4880.
[23] Z. Hu, Y. Xie, Y. Wang, L. Xie, G. Fu, X. Jin, Z. Zhang, Y. Yang, H. Wu, J. Phys. Chem. C 113 (2009) 12502–12508.
[24] L. Lv, P. Sun, Z. Gu, H. Du, X. Pang, X. Tao, R. Xu, L. Xu, J. Hazard. Mater. 161 (2009) 1444–1449.
[25] N. Takahashi, H. Hata, K. Kuroda, Chem. Mater. 22 (2010) 3340–3348.
[26] X. Fan, Z. Yang, R. Wen, B. Yang, W. Long, J. Power Sources 224 (2013) 80–85.
[27] X. Fan, Z. Yang, X. Xie, W. Long, R. Wang, Z. Hou, J. Power Sources 241 (2013) 404–409.
[28] R. Wang, Z. Yang, RSC Adv. 3 (2013) 19924.
[29] D.G. Evans, X. Duan, Chem. Commun. (Camb.) (2006) 485–496.
[30] Z. Luo, S. Sang, Q. Wu, S. Liu, ECS Electrochem. Lett. 2 (2012) A21–A24.
[31] J.L. Yang, Y.F. Yuan, H.M. Wu, Y. Li, Y.B. Chen, S.Y. Guo, Electrochim. Acta 55 (2010) 7050–7054.
[32] Y. Yuan, J. Tu, H. Wu, C. Zhang, S. Wang, X. Zhao, J. Power Sources 165 (2007) 905–910.
[33] T. Zhao, S. Chen, L. Li, X. Zhang, R. Chen, I. Belharouak, F. Wu, K. Amine, J. Power Sources 228 (2013) 206–213.